Salt-induced stress anomalies: an explanation for variations in seismic velocity and reservoir quality

Guido Hoetz[1,2,*], Joris Steenbrink[1], Niek Bekkers[3,4], Annemieke Vogelaar[3,5] and Stefan Luthi[3]

[1]*Nederlandse Aardolie Maatschappij B.V. PO Box 28000, 9400 HH Assen, The Netherlands*
[2]*Present address: Energie Beheer Nederland B.V. PO Box 19063, 3511EP Utrecht, The Netherlands*
[3]*Department of Geotechnology, Delft University of Technology, Stevinweg 1, 2628 CN Delft, The Netherlands*
[4]*Addax Petroleum Services Ltd, Avenue Eugène-Pittard 16, Genève, Switzerland*
[5]*N.V. Nuon Energy, PO Box 41920, 1009 DC Amsterdam, The Netherlands*
[*]*Corresponding author (e-mail: Guido.Hoetz@ebn.nl)*

ABSTRACT: Accurate rock property prediction is often a critical success factor for wells targeting hydrocarbons. This applies not only to reservoir porosity and permeability affecting productivity directly, but also to acoustic velocity, seismic time-to-depth conversion and depth prognosis. A detailed analysis of variation in the overburden rock velocity in the Southern North Sea has shown that Triassic velocity variations of up to 18% occur within short distances (e.g. <1 km). A correlation was found between increased acoustic velocities and the presence of an underlying salt weld. Salt Induced Stress Anomaly (SISA), a geomechanical model, is presented that can explain these observations and is based on the principles of buoyancy and point-loading. In the initial state, prior to salt movement, the vertical effective rock stresses resulting from the overburden weight are transmitted uniformly and cause laterally even compaction in the sediments. However, once the salt layer is able to flow and redistribute itself under the influence of buoyancy forces, the overburden stress will concentrate itself near the salt welds. This locally increased stress gives rise to higher velocities in the overburden. The same stress concentration model can also explain deterioration in the porosities of the Rotliegend reservoir as observed underneath salt welds.

KEYWORDS: *geomechanics, seismic velocities, depth conversion, velocity anomaly, salt, reservoir properties*

INTRODUCTION

In quantifying petroleum reserves, estimating correct reservoir rock properties, such as porosity, permeability and saturation, is imperative. However, depth estimates and depth uncertainties also play an important role, as these are key factors controlling the volumes of bulk rock and hydrocarbons-in-place. In the workflow leading to depth estimates, the seismic time-to-depth conversion (often simply referred to as depth conversion) is a paramount step (Robein 2003; Doornenbal 2001).

In depth conversion, a reflection – recorded in time – is translated into a surface in the depth domain. In this conversion process the seismic velocity (i.e. the speed at which the acoustic waves travel through the rocks) is required as input. Often each rock type has its own specific velocity which depends on many parameters, of which lithology and burial depth are among the most important (Al-Chalabi 2001). Under favourable conditions, seismic velocities can be derived from seismic reflection data (Hoetz & Pi Alperin 2009). Stacking velocities or migration velocities tend to be accurate for high quality shallow reflectors in the absence of anisotropy. However, these processing-derived velocities often lack the accuracy and resolution to describe the deeper layers sufficiently. In these cases, the depth conversion relies on velocities based on well data and empirically derived velocity functions (Robein 2003).

Incorrect velocity assumptions lead to errors in depth estimates and hydrocarbon volume estimates. In specific cases these errors can lead to disappointing well results, even to wells that end up dry (Fig. 1). This is also relevant in mature hydrocarbon provinces, such as the Southern North Sea, where remaining drilling targets are often characterized by relatively small gas or oil columns. As a consequence, those targets are very sensitive to depth prediction errors.

K07B102A is an example of such a well in the Dutch sector of the Southern North Sea as it encountered different rock properties than anticipated. This development well, drilled in 2003, encountered the Rotliegend reservoir porosity significantly lower than predicted (Fig. 2). However, more damagingly, it reached the reservoir some 100 m deeper than predicted and outside the specified uncertainty range of ± 50 m. As a result, the gas-bearing interval in the Rotliegend reservoir was limited to a few metres and completion of the well was uneconomic. A post-drilling review concluded that the depth error resulted from an unanticipated, strong lateral

DOI 10.1144/1354-079311-002

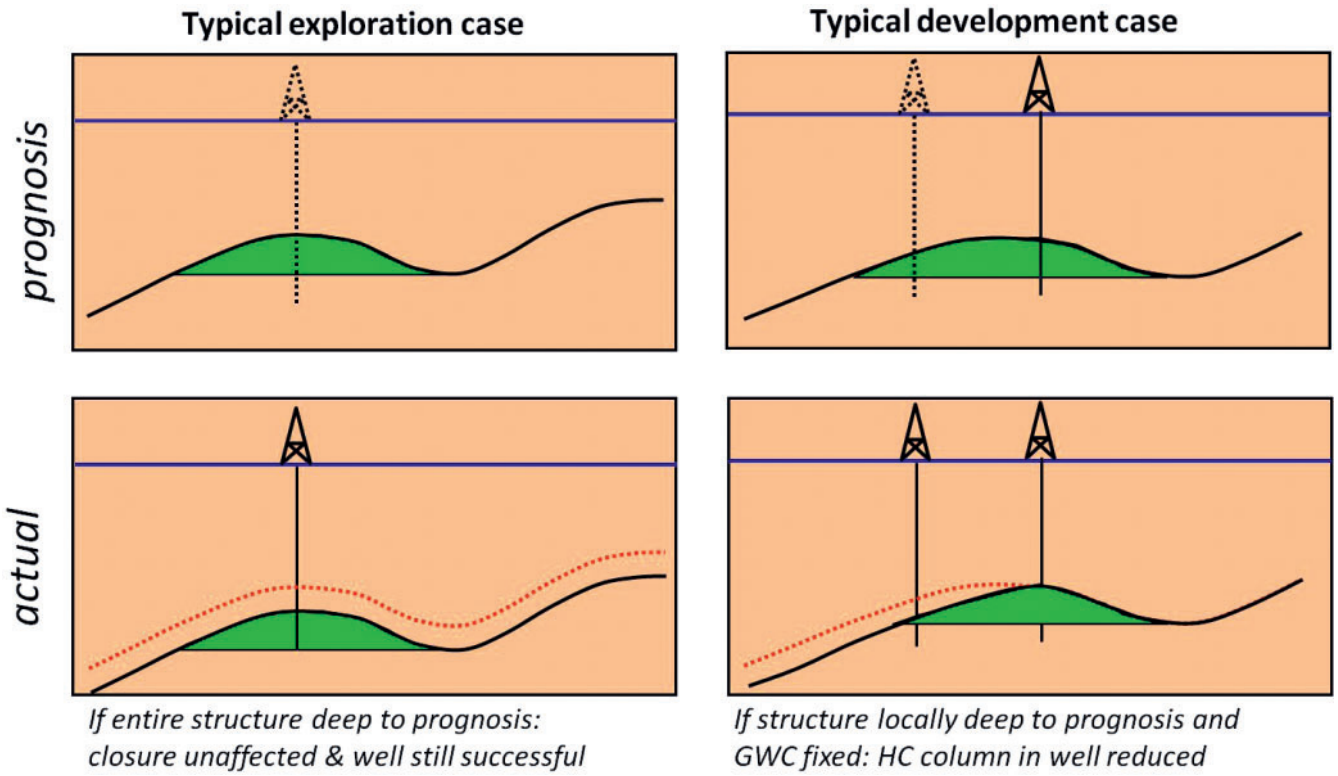

Fig. 1. Graphic illustration of potential impact of depth prognosis errors in seismic time-to-depth conversion. The consequences depend on the situation but can lead to a failed well. GWC, gas–water contact; HC, hydrocarbon.

velocity gradient in the Triassic part of the overburden (Hoetz 2005) of unknown origin. This triggered a further investigation into the nature, origin and distribution of this type of velocity anomaly. Improved understanding might lead to prediction of these anomalies and might help to avoid drilling dry wells in the future.

As a first step, the seismic processing velocities available for this area were reviewed. It became clear that these lacked the accuracy to detect such velocity anomalies and that they were not suited for improved depth prognosis. A better understanding of the nature of this anomaly was expected from an integrated geological/geophysical approach with the large available well database as a starting point.

SONIC VELOCITY ANALYSIS

In order to better understand the factors that control Triassic velocity distribution, existing, good quality sonic velocity data in K07 and surrounding blocks were analysed. Initially, the study area was limited to some 80 wells in an offshore concession of some 2500 km^2 (AOI 1 in Fig. 3; Bekkers 2005). At a later stage, the study area was increased to some 25 000 km^2 (AOI 2 in Fig. 3; Vogelaar 2006).

Subsequently, the existing Intra-Triassic stratigraphy in these wells was reviewed and quality controlled in detail to allow a velocity comparison of equivalent stratigraphic intervals. For the velocity analysis the data were subdivided into seven Triassic intervals (Table 1) using the following criteria:

- interval stratigraphic boundaries have to be clearly definable from the logs;
- intervals contain (largely) homogeneous lithology.

For all wells, the average interval velocity was calculated for each Triassic interval from the sonic log data. For AOI 1 (Fig. 3), these interval velocity control points served as input to generate velocity maps using convergent gridding in Petrel. These maps show the variability of the velocity, or more precisely: the layer average sonic velocity, for each interval. The velocity maps are constructed to identify the wells which have measured velocities that are out-of-trend. By way of example, the velocity of the Main Claystone member (RBSHM, the deepest interval) ranges from around 3000 m s^{-1} to as much as 4700 m s^{-1}. (Fig. 4a). This velocity variation is assumed to be the result of several controlling factors, some of which are well understood and can be estimated. By backing out the known effects, the residual velocity variations (i.e. anomalies) may become more pronounced.

Some of the velocity variability can be explained as being the result of variations in the depth of burial. Burial compaction is a well-known mechanism involving processes such as de-watering of sediments and lithification (diagenesis), causing the rocks to harden. Via empirical relationships, the effect of burial compaction can be modelled, allowing prediction of the velocity characteristics of a certain rock as a function of depth. These so-called velocity–depth trends have been described by Al-Chalabi (1997, 2001, 2002), Japsen (1993, 1998) and others. A commonly used velocity–depth trend function assuming linearity with depth has the following expression:

$$V(Z) = V_0 + KZ \quad (1)$$

where V is the instantaneous velocity, V_0 the normalized velocity (i.e. corrected for depth), K the vertical velocity gradient and Z the depth of the rock under consideration. This function was originally designed for a Tertiary basin setting, where monotonous deposition prevails. In such cases a simple linear regression of the sonic log response against depth suffices to derive the V_0 and K coefficients. This approach results in a single function describing the entire sediment

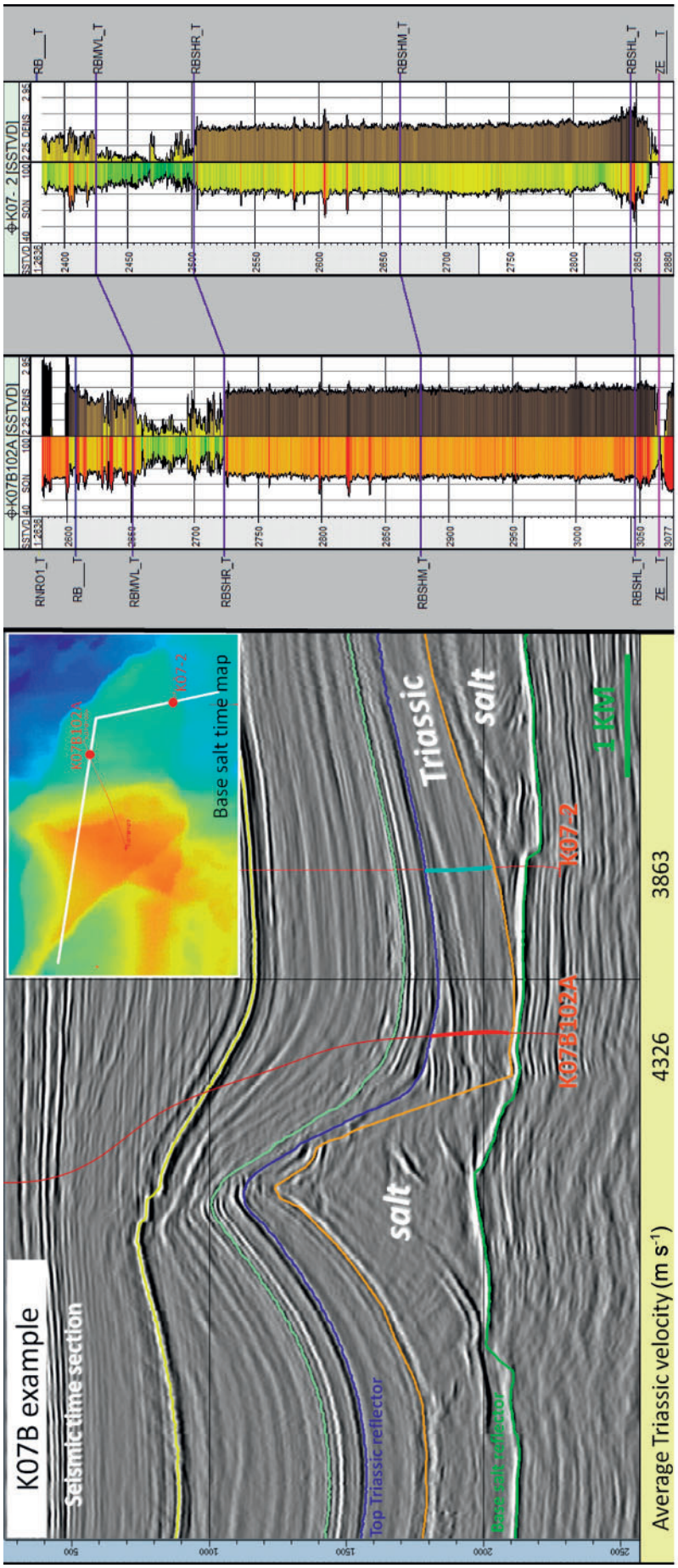

Fig. 2. (**a**) Seismic time section across well K07B102A and its close offset well K07–2. The base salt reflector (green) defines approximately the top Rotliegend Reservoir. (**b**) Sonic (SON) and density (DENS) log correlation of the Lower Germanic Triassic (RB) interval, flattened at the top Zechstein (ZE_T), illustrating faster and denser rock in K07B102A than K07–2. Well tops define unit boundaries. The average sonic velocities for the Triassic layer are listed in (a), below the wells.

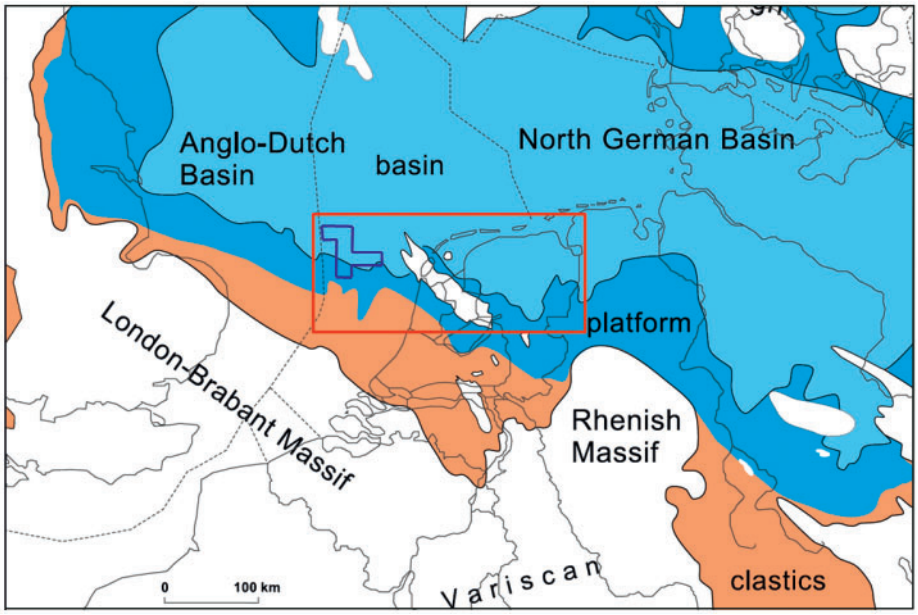

Fig. 3. Study outlines AOI 1 (blue) and 2 (red) plotted together with the present-day distribution and facies of the Zechstein (Z2 Carbonate, Late Permian) in the central and western part of the Southern Permian Basin (after Geluk 2007).

package. If the deposition varies in time and composition, the above method can be modified by splitting the interval into different layers. A best match of V_0 and K is thus derived for each layer separately.

As depth conversion of the deeper sequence (e.g. the Rotliegend reservoir) is the objective, there is no need to depth-convert every reflection precisely. As long as the layer boundaries are converted accurately, the layer-cake approach will result in a reliable depth map for the objective (Marsden 1989).

Under these conditions it is possible to estimate the parameters V_0 and K via linear regression of the layer average

Table 1. *Intra-Triassic layers used in the sonic velocity analysis; interval 1 is the deepest (oldest) interval*

Interval	Name	Abbreviation	Main lithology
7	Keuper Fm.	RNKP	Shale
6	Muschelkalk Fm. and top Röt Fm.	RNMU	Carbonates
5	Solling Fm. and Main Röt Evaporite Mb.	RNSO + RNROU	Evaporites
4	Volpriehasen Clay Mb., Hardegsen and Detfurth Fm.	RBM (excl RBMVL)	Sandstone and shale
3	Volpriehausen Sandstone Mb.	RBMVL	Sandstone
2	Rogenstein Mb.	RBSHR	Shale
1	Main Claystone Mb.	RBSHM	Shale

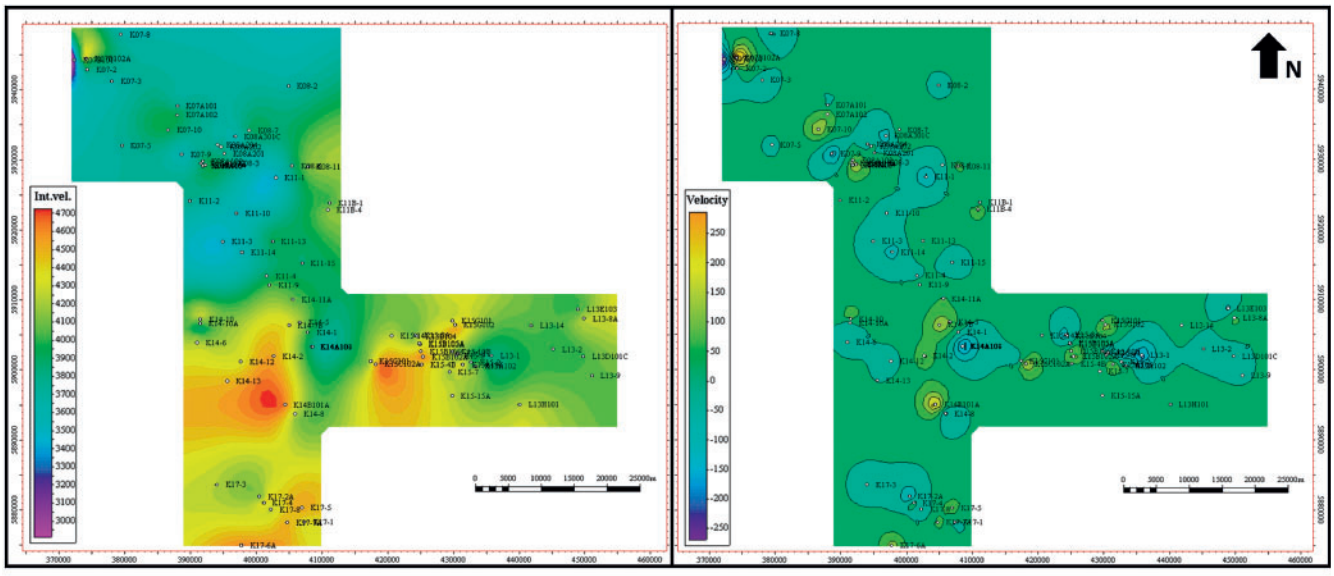

Fig. 4. Interval velocity maps: (**a**) actual velocities in m s^{-1} for interval 1 as measured by the sonic logs; (**b**) residual velocities after eliminating known depth effects and regional lateral trends.

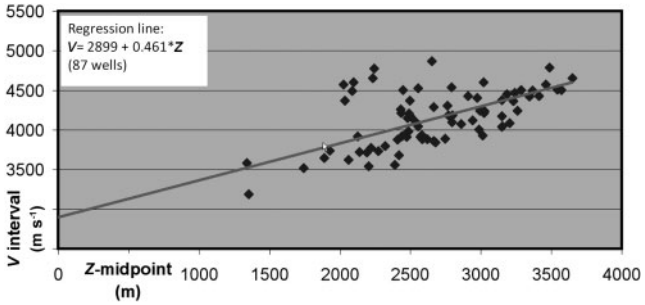

Fig. 5. Linear regression of interval velocity versus midpoint depth (layer 1).

velocity (V_{int}) vs. the midpoint depth of the layer (Z_{mid}) using the expression:

$$V_{\text{int}} = V_0 + KZ_{\text{mid}} \tag{2}$$

This method is easy to implement and the crossplot of V_{int} vs. Z_{mid} allows the applicability of the resulting linear relation to be quality controlled. An example of this regression analysis

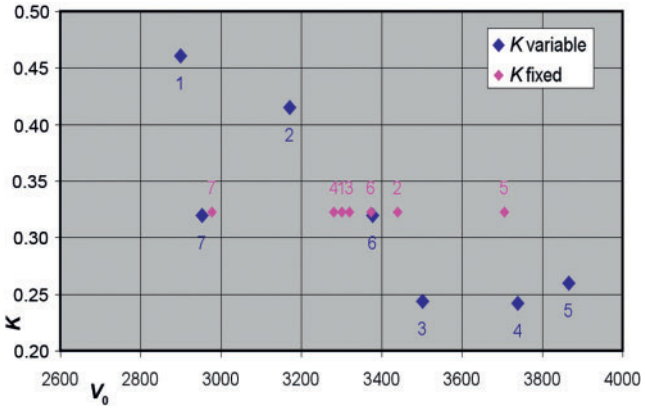

Fig. 6. Regression results for all seven Triassic layers. Blue: the V_0 and K parameters are optimized for each layer separately. Red: the V_0 values with K kept constant for all layers at 0.323 s^{-1}.

(Triassic interval 1, based on some 80 wells) is given in Figure 5.

The best fits for V_0 and K for all seven Triassic layers individually are represented graphically in Figure 6. The empirical relationships are seen to vary for the different units and are dependent on the lithology. In order to investigate how velocities vary for the different Triassic layers, the regressions have also been conducted with a single best-fitting (*global*) K value of $K = 0.323\ s^{-1}$. From this analysis it can be concluded that, after correcting for variations in burial depth, using the global K value, the fastest Triassic layer is the Röt Salt (L5), while the Keuper (L7) is the slowest layer.

It is also possible to calculate for each well the exact V_0 value that corresponds with the global K factor:

$$V_{0Wi} = V_{Wi} - KZ \tag{3}$$

where V_{0Wi} is the normalized velocity for well Wi, V_{Wi} the velocity for Wi, K is the global velocity gradient and Z the layer midpoint depth.

For each well the difference between the regression estimate (V_0) and the actual normalized velocity (V_{0Wi}) can be seen as the velocity residual for well Wi and is defined as:

$$\Delta V_{0Wi} = V_{0Wi} - V_0 \tag{4}$$

The ΔV_{0Wi} values are defined at the wells and can be gridded for the area of interest. After this normalization step, typically, the lateral variation in velocity due to burial depth differences has been reduced. The remaining velocity variation can partly be explained by lateral depositional facies changes and/or tectonic inversion, both effects that, in this setting, typically act on a large (horizontal) scale. Under this assumption the effects can be backed out by subtracting a smoothed version of this grid (i.e. eliminating the long wavelength information or applying a low-cut filter). In this way a velocity anomaly (dV_0) is obtained, which highlights the velocity gradients not accounted for (Fig. 4b).

Cross-plots of velocity anomalies of adjoining layers (Fig. 7) show a good correlation except for layer 5, the Röt salt, with layers 4 and 6, respectively. Thus, if, for example, the Main Claystone member (L1) has a high residual velocity, the

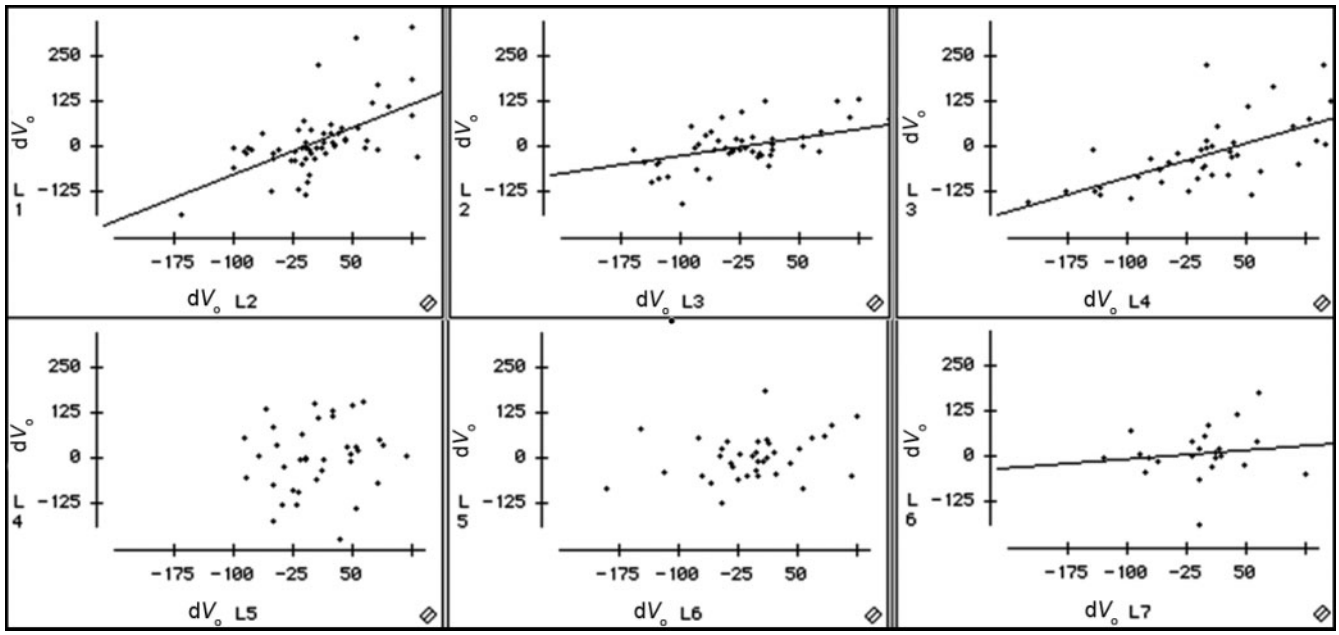

Fig. 7. Velocity anomaly cross-plots of adjacent layers. The correlations of the first four (deepest) layers are seen to be particularly good.

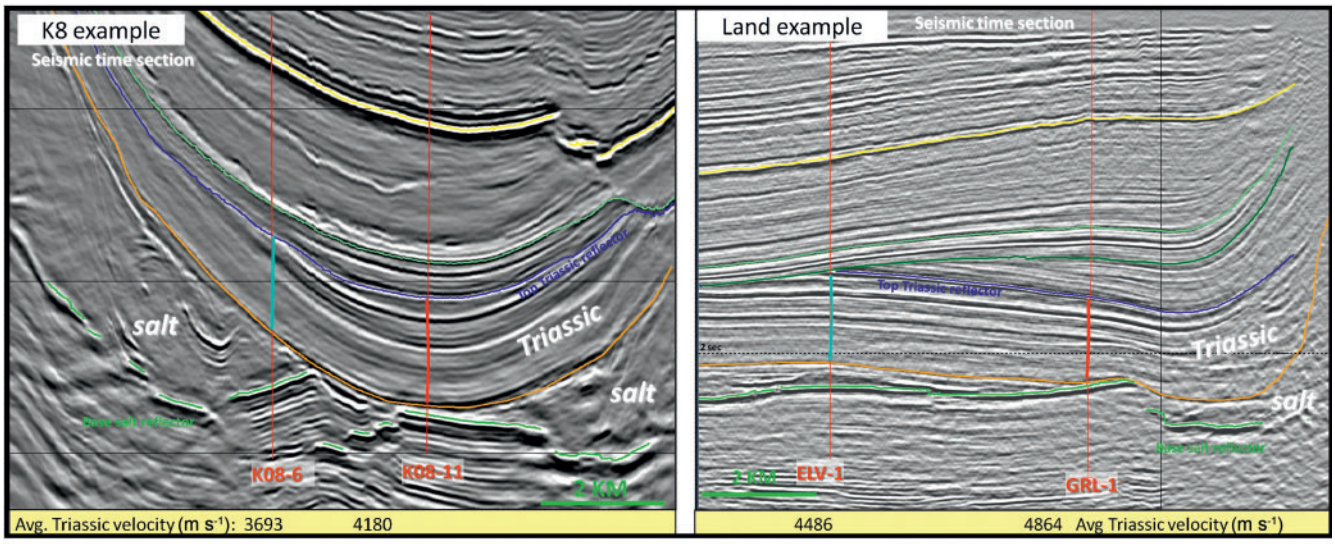

Fig. 8. Examples of wells where the Triassic velocity changes rapidly over short distances: (**a**) offshore block K08; (**b**) onshore Drenthe area. Fast Triassic is indicated in red, slow in blue. Average sonic velocities are listed below the boreholes. Wells in, or near, salt welds show higher velocities.

Rogenstein (L2) will also have a high residual velocity. By contrast, L5 has no correlation with the other layers, because salt has a fairly constant velocity.

INTERPRETATION OF RESULTS

Mapping of the Triassic sediment velocities in the study area AOI 1 (Fig. 3) shows significant lateral variability. Strong velocity gradients are identified around well K07B102A and in other areas. Part of this variability can be explained by the fact that certain wells contain more complete Triassic sections than others. Mapping of the velocities for intra-Triassic layers (Fig. 4a) also shows variability that is partly caused by variable depths of burial and depositional changes. After backing out these effects, the velocity anomalies for the wells can be analysed (Fig. 4b). Cross-plotting dV_0 for adjacent layers shows that the anomalies can be correlated. The anomalies are thus not confined to a particular layer: if, for example, layer 1 has an anomalously high velocity, then layer 2 is also anomalously fast (Fig. 7).

Origin of velocity anomalies

The velocity anomalies identified here affect, in particular, the deeper Triassic layers. Several mechanisms have been postulated to explain their origin:

1. cementation or leaching of the Triassic related to intra-Triassic faulting;
2. depositional variations linked to thickness variations of the Triassic members;
3. salt plugging of the Triassic beds related to piercing salt domes in their vicinity;
4. pore pressure variations.

These hypotheses have been evaluated using seismic displays that tie two wells to each other: one well that measures a relatively high Triassic velocity (positive anomaly) and a nearby offset well that shows lower velocities (negative anomaly) over the same Triassic section. By doing so, the subsurface geometries can be analysed to find a common explanation for the velocity gradients. It turns out that none of the above hypotheses can explain the observed anomalies. For example, the presence of Triassic faults as mappable from seismic data does not correlate systematically with the presence of anomalous velocities. The same applies to hypotheses 2 and 3. Hypothesis 4 is ruled out as all studied wells are effectively at normal hydrostatic pressure.

The seismic evaluation, however, identified a common factor in the layer geometries: it appeared that, in most cases, the wells with increased Triassic velocities were found at locations where the underlying Zechstein salt thickness was severely reduced or even fully absent. In addition to well K07B102A, this effect is seen in six other wells within study area 1; for example in well K08–6 (Fig. 8a).

Conversely and significantly, in the study set, there are no *negative* examples where wells without Zechstein salt show lower velocities compared to adjacent offset wells. These observations point to a correlation between the presence of a salt weld, i.e. an area of full salt withdrawal, and the occurrence of higher Triassic velocities.

The study area was subsequently extended to cover most of the northern Netherlands and the adjacent offshore area, the Dutch part of the Zechstein salt basin (AOI 2, Fig. 3). The same screening approach as previously applied resulted in 16 more examples of wells that were drilled in, or near, salt welds and where the Triassic sonic data show indications of increased velocities compared to offset wells (see Fig. A1 in Appendix A). A typical example is the onshore well GRL-1 (Fig. 8b).

The SISA model

The observation that increased velocities are typically found near salt welds points towards a geomechanical explanation. The combination of rigid rocks with mobile salt can give rise to point loading. On a geological time-scale, salt is considered to behave as a viscoelastic fluid (Christensen 1982). The Salt-induced Stress Anomaly (SISA) concept is best illustrated with simplified geometry using an analogue termed the 'brick-in-the-bathtub' model. As the density of the water (salt) is less than the brick (overlying rocks), the buoyancy forces support part of the weight of the brick, following Archimedes' principle. The remaining weight is supported by the contact area at the bottom of the bathtub. Figure 9 illustrates the two stages of this concept: the initial and the final geometry that lead to the

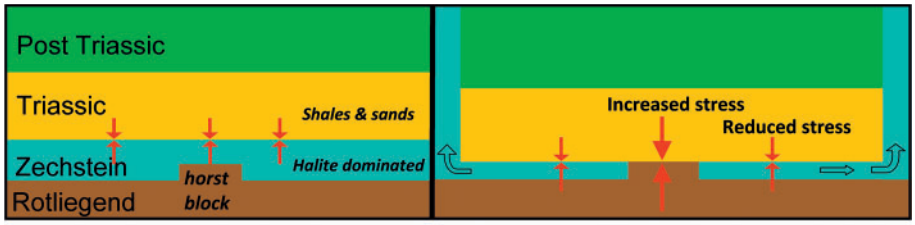

Fig. 9. The 'brick in the bathtub' model explains how stresses change following salt creep: (**a**) initial situation; (**b**) final situation. See text for explanation.

point-loading and thereof the stress anomaly. The figure is a cross-section through a 3D model. Initially the salt layer is sufficiently rigid to support the entire overburden uniformly (Fig. 9a). The vertical stresses are equal and hence the Triassic velocities are laterally constant. The pre-salt topography is, in this case, irrelevant for the post-salt stresses. With increased burial and geological time, the salt will get squeezed out laterally and move upwards in the form of diapirs (Fig. 9b). This causes the overburden to subside until an obstacle, such as a horst block, is encountered. The overburden weight will thus be carried primarily by the horst block, since locally the salt is absent and a salt weld has developed. Above the salt weld, the vertical rock stress will increase compared to the adjacent areas, resulting in higher acoustic velocities caused by increased compaction, cementation and de-watering. Based on this simple model, it is expected that the vertical SISA is largest just above the weld and decreases in magnitude horizontally and vertically away from the weld.

Analytical model: 'brick-in-the-bathtub'

Stress calculations for arbitrary geometries are generally carried out using Finite Element methods and require many input parameters. However, a simplified model such as the 'brick in the bathtub' can be described using basic equations from mechanics. The brick embodies the rigid overburden block (e.g. Mesozoic sediments), while the bathtub fluid represents for the mobile salt. The bathtub itself has an irregular base (e.g. a horst block). This analogue helps, as a first approximation, to understand what parameters play a significant role in the SISA effect. Based on this model it is expected that the magnitude of the stress anomaly above the salt weld is a function of the:

- density contrast between the overburden block and the salt;
- areal size of the salt weld;
- areal size of the brick;
- height of the brick;
- height of the salt diapir which is controlling the salt pressure.

An estimate of the stress increase just above the weld (at P1 in Fig. 10) is now derived via a simplified mechanical model, with the proviso that not all aspects of salt-induced stress distributions (e.g. stress arching) are represented fully. An overburden block of finite horizontal cross-surface area (A) and height (H) will be considered. The density of this overburden block is ρ_{ov} and the gravity constant is given by g.

The total force exerted by the mass of the overburden block is given by:

$$F_{ov} = \rho_{ov} A H g \tag{5}$$

In case 1 (initial situation: salt layer rigid and continuous), the weight is uniformly carried by the underlying rigid salt. The pre-salt topography shows a small high (horst) in the middle. The vertical stresses in the brick at P1 (above the horst) and P2 (away from the horst) are equal and are controlled by the mass of the overburden using the expression:

$$\sigma_{ini} = \rho_{ov} H g \tag{6}$$

In case 2 (salt mobilized and re-distributed), the weight of the overburden is partly supported by the salt and partly by the horst (with surface area B). The following balance of forces applies:

$$F_{ov} = F_{horst} + F_{salt} \tag{7}$$

Knowing the salt pressure (σ_s), the upwardly directed force F_{salt} is given by:

$$F_{salt} = \sigma_s (A - B), \tag{8}$$

in which, following Pascal's principle (and ρ_s= salt density) the (isotropic) stress is given by:

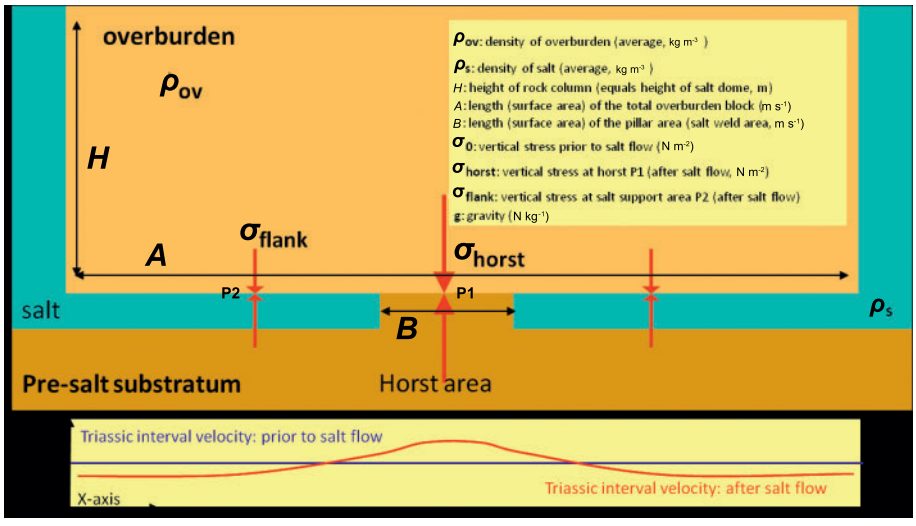

Fig. 10. Representation of the 'brick in the bathtub' model annotated with parameters used in the above analysis. The stress anomaly results in a velocity anomaly in the Triassic as depicted schematically underneath.

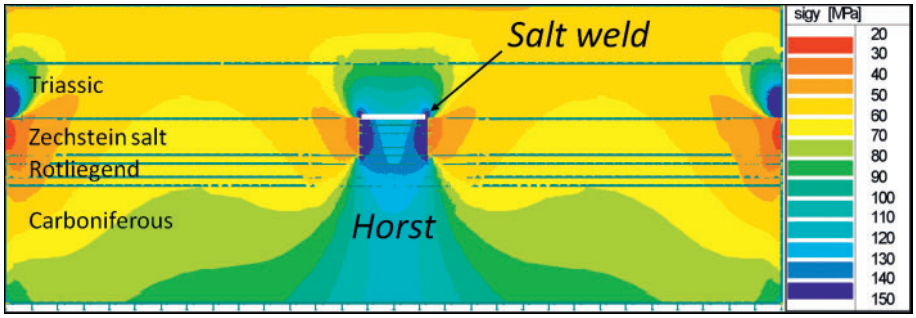

Fig. 11. FEM cross-section showing the modelled vertical stress distribution as a result of the salt weld. Blue indicates increased vertical stresses. Strong stress variations at the edges are artefacts in the modelling and not significant for this study.

$$\sigma_s = \rho_s H g \tag{9}$$

(Note that, in this model, the salt is regarded as a continuous liquid phase to the surface (with height = H) and can be seen as providing a buoyancy force to the brick. In case $B = 0$ this force follows directly from Archimedes' principle.)

F_{horst} can be solved by combining equations (5), (7), (8) and (9) to yield:

$$F_{horst} = Hg(\rho_{ov}A - \rho_s A + \rho_s B) \tag{10}$$

The vertical stress in the horst ($\sigma_{horst} = F_{horst}/B$) is given by:

$$\sigma_{horst} = Hg(\rho_{ov}A/B - \rho_s A/B + \rho_s) \tag{11}$$

The stress anomaly ($\sigma_a = \sigma_{horst} - \sigma_{ini}$) as a result of the salt weld is given by:

$$\sigma_a = Hg\Delta\rho([A/B] - 1) \tag{12}$$

in which is $\Delta\rho = \rho_{ov} - \rho_s$.

With some assumptions, an estimate of the stress anomaly can be made for this model. From the seismic data around K07B102A (not shown here) one can *guestimate* the following dimensions: a 3 km thick rock slab (brick) of 5 × 4 km residing on a salt weld of 500 × 500 m (i.e. A/B = 80), with an overburden density of 2500 kg m^{-3} and salt density of 2100 kg m^{-3}. With this input value, expression (12) calculates a stress anomaly of 97 MPa (970 bar). This stress increase, resulting from the point-loading, is on top of the normal rock stress (stage 1) of 73 MPa.

This simplified model ignores deformation and offers only a first pass approximation of the stresses immediately above the salt weld. In order to evaluate the stresses quantitatively away from this area, more complex analysis is required. Boussinesq (1885) solved the problem of stress produced at any point in homogeneous, elastic medium as the result of a point load. More generic methods are based on Finite Element geomechanical modelling (e.g. Fredrich *et al.* 2003; Sengupta & Bachrach 2008).

Numerical model

In reality, rocks have finite shear elastic moduli and hence shear stress and, therefore, deformation needs to be accounted for. This introduces complications for the analysis but does not alter the basic concept that stress concentration around the salt weld will occur. The simplified stress anomaly calculated analytically (above) is applicable to the contact of horst and overburden.

In order to evaluate the stresses away from this area, methods based on Finite Element Modelling (FEM) can be used. ESA-Prima WIN is a tool utilized mainly by civil engineers to conduct structural analysis. It uses a 2D-H approach, i.e. it builds two-dimensional quadrilateral models with a certain height (Vogelaar 2006).

The model built here consists of eight layers. For every layer the following rock properties were specified: density, Young's modulus and Poisson's ratio, together with the geometric properties – thickness, length of the overburden rock slab and length of the weld. The model allows for parameters to be varied and the results investigated in terms of stress response. An example of the resulting stress anomaly distribution is given in Figure 11. For the tested assumptions on properties and geometries, the vertical stresses obtained are up to 150 MPa (Vogelaar 2006). The stress prior to salt weld formation is calculated to be 73 MPa, implying that the stress increase (anomaly) is 77 MPa. This FEM model suggests, therefore, that the SISA effect approximately doubles the vertical stresses locally. Such enormous stress increases are probably unrealistic, as differential vertical stresses of this magnitude are likely to cause rupturing or fracturing of the rocks depending on the Mohr–Coulomb failure criteria for the rocks in question. The resulting deformation effects are not modelled here.

According to the FEM model, in the area adjacent to the salt weld, values below 73 Mpa (i.e. negative stress anomalies) are obtained. This effect is plausible as positive vertical stresses have to be compensated by negative stresses due to stress-arching.

It seems possible that certain offset wells in the cases evaluated (Appendix A), for which sonic logs were used as reference, are actually positioned in a zone with a negative stress anomaly. Obviously the result is a strong lateral velocity gradient between the *stressed* well (i.e. a well positioned in an area with a positive vertical stress anomaly) and the *arched* well (i.e. a well positioned in an area with a negative vertical stress anomaly).

Well data model

An alternative way to quantify the magnitudes of the stress anomaly is based on the sonic velocity measurements. The velocity–depth trend analysis shows that the Triassic velocities have a depth dependency (Japsen 1993; Al-Chalabi 2001). Increased depth represents larger effective rock-stress, following the equation:

$$\sigma = \rho_{ov} H g \tag{13}$$

Combining this with the empirical V_0-K relation (equation (1), using $H = Z$) allows estimation of the stress from the sonic velocity:

$$\sigma = (\rho_{ov} g/K)(V - V_0) \tag{14}$$

Using the above general stress versus velocity relationship, it is possible to link the velocity anomaly to the stress anomaly:

$$\Delta\sigma = c\Delta V \tag{15}$$

in which $\Delta V = V - V_0$, $c = \rho_{ov} g/K$. Assuming: ρ = 2500 kg m^{-3}, g = 9.8 m s^{-2} and K = 0.323 s^{-1} yields c = ~ 76 × 10^3 N m^{-3} s.

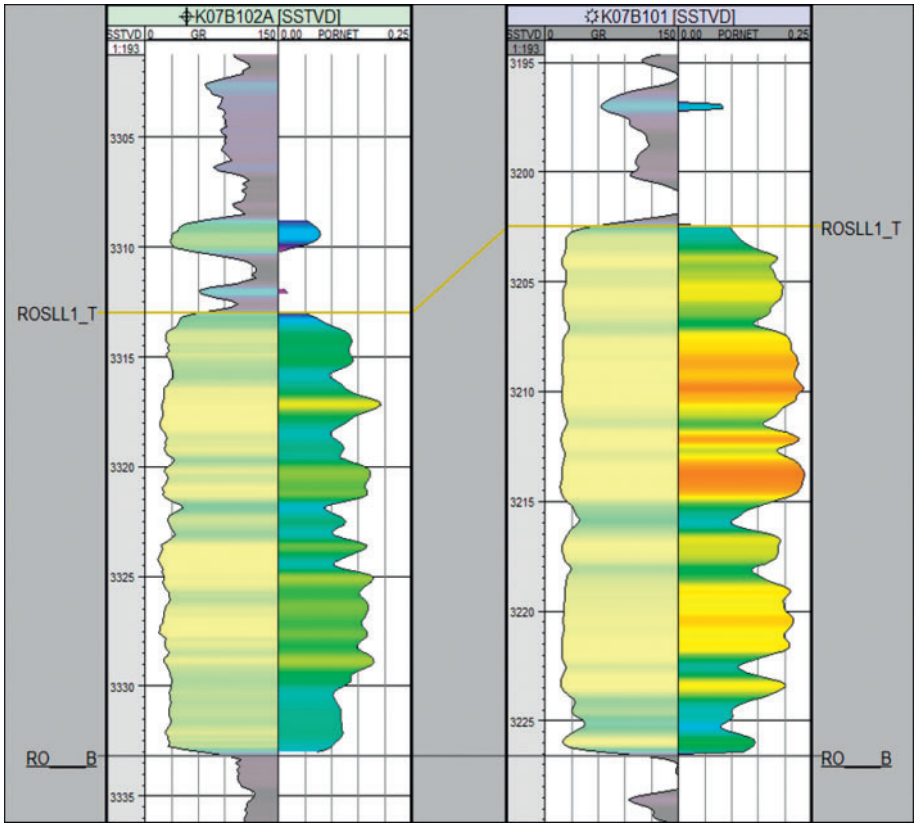

Fig. 12. Reservoir section logs showing porosity reductions below the salt weld. The 'stressed' well K07B102A shows a significantly reduced porosity (4 porosity units) for the main Rotliegend layer (ROSLL1) compared to offset well K07B101. The reduction in thickness, as indicated by the log, might also be related to the stress anomaly.

For well K07B102A, where the velocity anomaly is 463 m s^{-1} (Fig. 2; velocity difference between the *stressed* and the offset well), the corresponding stress anomaly thus amounts to 35 MPa. The resulting stress effect is equivalent to an additional burial depth of some 1400 m. The difference between the modelled stress anomaly using FEM (77 MPa) and the stress anomaly calculated from well data (35 MPa) can be explained in several ways.

1. The FEM approach used does not take into account the possibility of rock failure and changes in the layer geometry which would reduce the modelled stress anomaly.
2. The FE model geometries are overly simplified and do not take into account the specifics of well K07B102A.
3. The input parameters in the models, particularly the rock properties, are poorly defined and, therefore, have a large uncertainty.
4. K07B102A was not drilled through the centre of the salt weld, i.e. the area with maximum stress. In fact it penetrated a few metres of salt, suggesting that the actual salt weld is nearby. The seismic data indicate that the salt weld centre is, at most, a few hundred metres away from the well.

Both above-stress-anomaly estimates are lower than those calculated for the 'brick in the bathtub' model (97 MPa). The latter model is introduced mainly for further illustration of the concept and is known to fall short in realistic rock geomechanical modelling as deformation, for example, is not included.

Stresses below the salt weld

Most Rotliegend traps are covered by salt which constitutes the top seal for the accumulation. Nevertheless, there are also cases where hydrocarbons are successfully trapped below salt welds. The FEM model (Fig. 11) indicates that the area of increased stress is not only found above the salt weld, but also below it. If stress concentration also occurs below salt welds, it should have consequences for the reservoir properties and thus well productivities. In particular, rock porosity is known to be a function of effective rock stress. In order to test this hypothesis, the porosities of the Rotliegend reservoir were analysed. For those wells drilled through, or near, a salt weld, the layer-average Rotliegend sandstone porosities were compared with those from nearby offset wells beyond the salt weld. For well K07B102A, which appeared strongly affected by the SISA effect, a comparison with offset reference wells indicated a porosity reduction of 2–4% (Fig. 12).

In the majority of the other cases there is evidence that the stressed wells show reduced porosities compared to the reference wells. Typically, the porosity reduction amounts to 1–3%, a significant reduction for the main Rotliegend reservoir units where porosities average around 15%.

In some cases, there are also indications that the porosity reductions as a result of SISA lead to reduced permeabilities and hence reduced well flow rates. The SISA diagenetic effects are comparable to the effects from tectonic inversion: a reservoir that was once buried deeper has typically poorer reservoir qualities compared to reservoirs with a monotonic burial history. However, the stress disturbances from SISA are more complex than from simple overburden loading. The point loading of SISA leads to significant differential stresses and could cause widespread fracturing both above and below the contact. There are, in fact, indications from layers underneath salt welds that show increased permeabilities that are likely related to fracture networks.

An additional complicating factor is *time*. It seems likely that the diagenetic effects resulting from SISA will have some time dependency: the longer a certain stress increase is active, the more diagenetic processes have the opportunity to affect reservoir quality in a detrimental way.

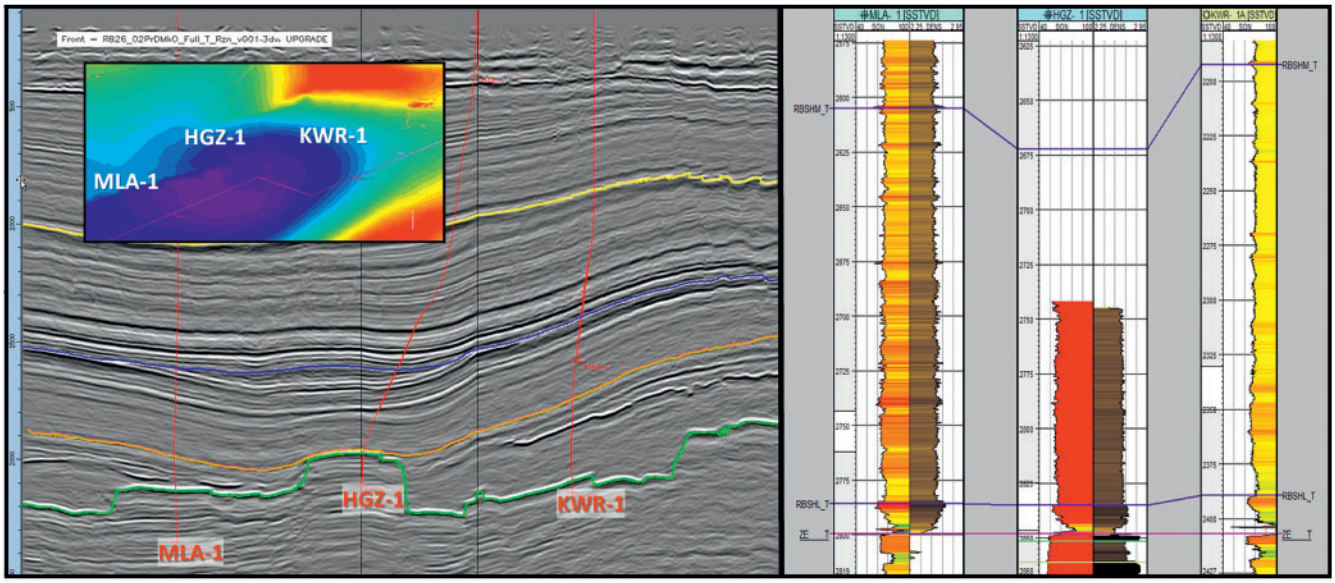

Fig. 13. (**a**) Seismic line showing the salt weld at the HGZ-1 location. (**b**) The Triassic has been partially logged and the sonic (left log) shows compressional velocities that are faster by 18% compared with the offset wells MLA-1 and KWR-1.

Predictions of SISA

In 2009, the Hoogezand well (HGZ-1) was drilled in the northeast of the Netherlands (Fig. 13) to appraise the western block of the Zuidlaardermeer structure, situated at the periphery of the Groningen gas field (Doornenbal & Stevenson 2010). The seismic data showed the Rotliegend to be situated under a salt weld and, therefore, a certain SISA effect was anticipated. The depth prognosis for HGZ-1 was adjusted 50 m downwards based on the experience in other SISA wells and it was decided to gather velocity information by running a sonic log over the Triassic section. As per prognosis, no salt was encountered and, importantly, the underlying reservoir was found to be gas-bearing. However, the reservoir depth was, despite the SISA adjustment, 30 m deeper than prognosed. The sonic log could be run only over the lower part of the Triassic due to poor hole conditions (possibly caused by a stress anomaly). Across the logged interval the sonic log consistently shows about 18% higher compressional velocities than in offset wells (Fig. 13). This velocity increase accounts for a depth error of about 70 m and compares well with the observed depth mismatch of 80 m, of which 50 m was anticipated. The porosity logs revealed that the reservoir in HGZ-1 is relatively tight, with average porosities of 9.2% compared to 11.7% in the offset well (Fig. 14). This effect is in line with the prognosed reduction in rock properties from the SISA model.

In order to increase the understanding of the SISA effect, several areas of further research have been suggested.

1. The velocity anomalies have been studied mainly using sonic data. In many wells checkshot/VSP (vertical seismic profile) data are also available. The inclusion of these sources of velocity information should increase the dataset for analysis.
2. The current analysis had been limited to the Triassic. Although the SISA model predicts that the effects are most pronounced near the salt weld and the Triassic often overlies the salt weld directly, there is no reason why other strata should not also be affected by the SISA effect.
3. Salt welds do occur in many basins around the world and the authors have seen examples from Oman, Gabon, Kazakhstan and offshore Brazil where SISA might be applicable. Extending the analysis to other basins should be very useful to gain further insights.
4. The FEM modelling conducted here is based on many simplifications. It is recommended that more realistic geometries are included and that sensitivities on the parameters be tested. Also, further investigation is merited regarding whether the Mohr–Coulomb failure criteria are applicable. The study of fractures from, for example, image logs in SISA wells might improve the understanding of permeability distribution and production behaviour.

The SISA concept presented here is based on the observed correlation between salt welds and stress effects and assumes that salt welds cause stress anomalies. Although this causality is made plausible here, it is not yet proven. Alternatively, it could be that stress anomalies initiate the formation of salt welds leading to the same correlations. Further geological work is required to prove the causality assumed here.

CONCLUSIONS

Errors in seismic velocity estimates result in incorrect reservoir depth estimates and can lead to unsuccessful wells. Generally, velocity variations can be related to variations in depositional facies and to diagenesis linked to the depth of burial. In the Triassic of the Southern North Sea rapid lateral variations in acoustic velocity have been identified that cannot be explained in these ways. A correlation was found between (sonic) velocities and a common factor in the structural setting. It appears that wells that were drilled at, or near, Zechstein salt welds tend to show higher velocities compared to offset wells where salt is present. This observation allows prediction of (and correction for) certain velocity anomalies directly from subsurface geometries visible on seismic data.

A simple geomechanical model based on buoyancy and point-loading can be used to explain the observations. In the SISA (Salt-induced Stress Anomaly) model, the salt weld acts as an area where vertical stresses are being concentrated and point-loading occurs. The effective stress increase leads to an

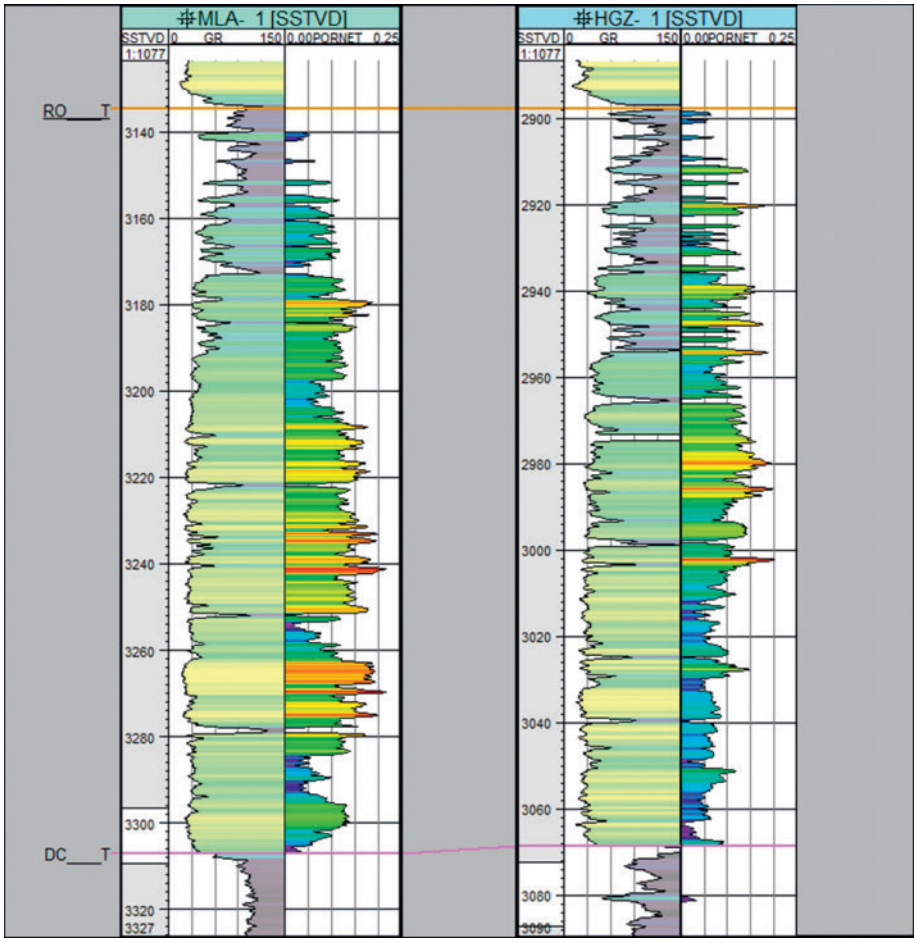

Fig. 14. Porosity logs (right) of the Rotliegend in wells HGZ-1 and MLA-1. The stressed well HGZ-1 shows a 2.5 porosity units reduction.

increased velocity through compression and enhanced diagenesis. The velocities can increase locally up to 18% and depth prediction errors of up to 80 m have been observed. Stress increase effects can also be identified below the salt weld. As a result, the porosities can be reduced by 1–4% (porosity units). The anisotropic stress distortion resulting from SISA might also lead to fracturing and hence permeability increase.

The SISA stress anomaly for well K07FA102 has been estimated quantitatively in three ways: (1) a simple analytical model; (2) FEM; and (3) applying empirical velocity–stress relationship. These methods yield maximum vertical stress increases ranging from 35–97 MPa which is significant if compared with the normal rock stress of 73 MPa for a comparable (SISA-free) situation.

Occurrences of anomalous velocities have also been interpreted as an expression of exhumation (Hillis 1995) or pore pressure anomalies (Japsen 1999). SISA is another geomechanical effect that should be taken into account when interpreting velocity distributions.

This paper merely documents the effect on velocities, porosities and permeabilities. It thus forms the basis for further investigation that takes into account the full 3D geometries and the appropriate geomechanical parameters in order to make better predictions of reservoir depths and qualities.

APPENDIX A

In total, 25 cases were selected to analyse and quantify the SISA effect (Fig. A1). Each case consists of a candidate SISA well (i.e. potentially SISA-affected well) plus one or more reference wells that are (likely) not affected by SISA but which have sonic data for comparison.

Each case is selected on the following criteria:

1. candidate well shows less than 100 m of Zechstein halite thickness;
2. 3D seismic data are available covering the candidate well and should indicate salt weld in near vicinity (less than 300 m away);

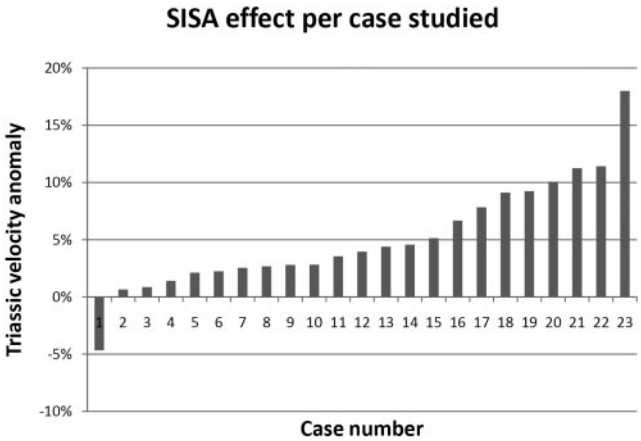

Fig. A1. Barchart showing magnitude of the Triassic velocity anomaly (in %) for all wells selected in this study (using the criteria mentioned in Appendix A).

3. nearby reference well(s) show significantly more Zechstein halite;
4. reliable sonic logs exist over the (Lower) Triassic section – for both candidate and reference wells.

The sonic response is checked against check shot data where available. The Triassic velocity anomaly (dV) is calculated by taking the difference in Triassic velocity between the candidate well and the (average) of the reference wells. In order to correct for depth differences: all velocities have been normalized using $K = 0.32\ s^{-1}$. The sonic SISA effect is calculated by taking dV and dividing it by the Triassic velocity of the candidate well. From the 25 wells, two wells were discarded because of unreliable sonic (cased hole logging). For one well a negative SISA effect (–4.7%) was measured. A possible explanation is that, for this well, which still logged 77 m of halite, the distance to the (postulated) salt weld might be too large and this well is actually not within the SISA area (not analysed further).

The authors would like to thank NAM, Shell, ExxonMobil, EBN, Wintershall, Oranje-Nassau and NUON for their permission to publish this material. Furthermore, special thanks to John Verbeek, Bas Spaargaren, Alice Post, Juan Pi Alperin and Anthony Mossop who have helped in shaping the ideas presented here. The concept of SISA and the method to estimate its magnitude quantitatively has been patented by Shell under the title 'Identifying a stress anomaly in a subsurface region' (TS 9559 by G. Hoetz).

REFERENCES

Al-Chalabi, M. 1997. Parameter non-uniqueness in velocity versus depth functions. *Society of Exploration Geophysicists*, **62**(3), 970–979.

Al-Chalabi, M. 2001. The use of instantaneous velocity in uplift investigations, *Geophysical Prospecting*, **49**, 645–655.

Al-Chalabi, M. & Rosenkranz, P.L. 2002. Velocity–depth and time–depth relationships for a decompacted uplifted unit. *Geophysical Prospecting*, **50**, 661–664.

Bekkers, N.B.M. 2005. *Cause and control of Triassic sonic velocity variations in the Southern North Sea*. MSc thesis, Section for Applied Geology, TU Delft, AES/AW/05-11.

Boussinesq, M. 1885. *Application des potentiels à l'' étude de l'' équilibre et du mouvement des solides élastiques, principalement au calcul des deformations et des pressions que produisent, dans ces solides, des efforts quelconques exercés sur und petite partie de leur surface ou de leur intérieur;memoire suivi de notes étendues sur divers points de physique mathématique et d'analyse*. Gauthier-Villars, Paris.

Christensen, R.M. 1982. *Theory of Viscoelasticity*. Dover Publications, Mineola, N.Y.

Doornenbal, J.C. 2001. *Regional velocity models of the Netherlands territory*. Paper A08. *In: Expanded Abstracts, 63rd EAGE Conference*.

Doornenbal, J.C. & Stevenson, A.G. (eds). 2010. *Petroleum Geological Atlas of the Southern Permian Basin Area*. EAGE, Houten.

Fredrich, J.T., Coblentz, D., Fossum, A.F. & Thorne, B.J. 2003. *Stress perturbations adjacent to salt bodies in the Deepwater Gulf of Mexico*. Paper SPE 84554, presented at the Proceedings SPE Annual Technical Conference and Exhibition.

Geluk, M. 2007. Permian in geology of the Netherlands. *In:* Wong, T., Batjes, D.A.J. & De Jager, J. (eds) *Geology of the Netherlands*. Royal Netherlands Academy of Arts and Sciences, Amsterdam, 63–83.

Hillis, R.R. 1995. Quantification of Tertiary exhumation in the United Kingdom southern North Sea using sonic velocity data. *American Association of Petroleum Geologists Bulletin*, **79**, 130–152.

Hoetz, G. 2005. *Salt induced stress-arching controlling rock properties*. Abstract presented at the American Association of Petroleum Geologists Conference, September 2005, Paris, France.

Hoetz, G. & Pi Alperin, J. 2009. *SISA seismically spotted: Salt Induced Stress Anomalies causing depth conversion errors now detected on Long Cable PSDM*. Extended abstract presented at the EAGE Conference, June 2009, Amsterdam, The Netherlands.

Japsen, P. 1993. Influence of lithology and Neogene uplift on seismic velocities in Denmark: implications for depth conversion of maps. *American Association of Petroleum Geologists Bulletin*, **77**, 194–211.

Japsen, P. 1998. Regional velocity–depth anomalies, North Sea Chalk: a record of overpressure and Neogene uplift and erosion. *American Association of Petroleum Geologists Bulletin*, **82**, 2031–2074.

Japsen, P. 1999. Overpressured Cenozoic shale mapped from velocity anomalies relative to a baseline for marine shale, North Sea. *Petroleum Geoscience*, **5**, 321–336.

Marsden, D. 1989. Layer cake depth conversion. *In: The Leading Edge of Exploration*, **8** (1), 9–14. SEG, Tulsa.

Robein, E. 2003. *Velocities, Time-Imaging and Depth-Imaging in Reflection Seismics: Principles and Methods*. EAGE, Houten.

Sengupta, M. & Bachrach, R. 2008. Velocity updating around salt bodies using stress modeling solutions and non-linear elasticity. *SEG Expanded Abstracts*, **27**, 3048.

Vogelaar, A. 2006. *Analysis of salt-induced stress anomalies*. MSc thesis, Section for Applied Geology, TU Delft, AES/AW/06-04.

Received 10 January 2011; revised typescript accepted 14 July 2011.